Fuel 306 (2021) 121641

Contents lists available at ScienceDirect

Fuel

journal homepage: www.elsevier.com/locate/fuel

Full Length Article

Ethane dehydrogenation over the single-atom alloy catalysts: Screening out the excellent catalyst with the dual descriptors

Yuan Zhang [a,b], Baojun Wang [a,b,*], Maohong Fan [c,d,e], Debao Li [f], Riguang Zhang [a,b,*]

[a] State Key Laboratory of Clean and Efficient Coal Utilization, Taiyuan University of Technology, Taiyuan 030024, Shanxi, PR China
[b] Key Laboratory of Coal Science and Technology (Taiyuan University of Technology), Ministry of Education, Shanxi, PR China
[c] Departments of Chemical and Petroleum Engineering, University of Wyoming, Laramie, WY 82071, USA
[d] School of Civil and Environmental Engineering, Georgia Institute of Technology, Atlanta, GA 30332, USA
[e] School of Energy Resources, University of Wyoming, Laramie, WY 82071, USA
[f] State Key Laboratory of Coal Conversion, Institute of Coal Chemistry, Chinese Academy of Sciences, Taiyuan 030001, Shanxi, PR China

ARTICLE INFO

Keywords:
Ethane
Catalytic dehydrogenation
Single atom alloy
Catalyst screening
DFT calculations

ABSTRACT

Single atom alloys (SAAs) catalysts become potential to provide excellent activity, selectivity, and stability toward the selective dehydrogenation of light alkanes by activating the desired C–H bond, however, the ideal metallic combination to best catalyze C_2H_6 dehydrogenation is unclear yet. In this study, the activity and selectivity of ethane dehydrogenation on fifteen types of SAA catalysts (Co, Ir, Ni, Pd and Pt doped-Cu, Ag and Au) were fully investigated using DFT calculations and microkinetic modeling, and compared with that on the widely reported Pd, Pt, Cr and Pt_3Sn. The results show that the activity of C_2H_6 dehydrogenation to gas phase C_2H_4 on all considered SAA catalysts has a relationship with C_2H_4 desorption energy, the easier the desorption of C_2H_4 is, the lower the activity of C_2H_6 dehydrogenation to gas phase C_2H_4 is. Similarly, C_2H_4 selectivity has a relationship with C_2H_5 adsorption energy, the weaker C_2H_5 adsorption energy is, the higher C_2H_4 selectivity is. Essential reason was explained based on the analysis of electronic properties. Thus, the dual descriptors, C_2H_4 desorption energy and C_2H_5 adsorption energy, were proposed to evaluate the activity and selectivity of C_2H_6 dehydrogenation to gas phase C_2H_4, respectively. Among these SAA catalysts, the low cost NiCu catalyst with the best activity and selectivity toward gas phase C_2H_4 formation is screen out, which is superior to the noble metals Pd and Pt widely reported. This study is expected to provide a simple and valuable method to screen out high performance SAA catalysts in alkane dehydrogenation to alkene.

1. Introduction

Nowadays, ethylene is mainly produced through the thermal steam cracking of naphtha and ethane; however, it suffers from the energy-intensive and coking problems [1,2]. Consequently, extensive attention was paid to developing alternative processes, one is the oxidative dehydrogenation (ODH) [3–5], and the other is the catalytic dehydrogenation (CDH) [6–8]. ODH occurs at low temperatures and suppresses the formation of hydrogen as a byproduct, while the selectivity issue becomes significant since the competition between the oxidative dehydration reaction and the very fast combustion of alkene product. Whereas CDH occurs at lower temperatures compared to the steam cracking, and thus lowers coke formation; moreover, the combustion is not concerned due to the absence of the oxygen, the dehydrogenation process can also produce H_2 [9,10]. Despite above advantages of CDH, it still requires high temperature (>700 K) and it is strongly endothermic.

Nowadays, the dehydrogenation of light alkane on the supported Pt catalysts exhibited excellent activity, selectivity, and thermal stability [11–13], however, the alkene from the dehydrogenation can strongly interact with Pt surface, weakening the desorption capacity of alkene and facilitating its deep dehydrogenation or C–C bond cleavage leading to surface carbonaceous species [14–16]. Thus, the pure Pt catalyst is rapidly deactivated due to large deposits of coke. Further, alloying Pt with Sn inhibits the catalyst deactivation and coke formation compared to the pure Pt catalyst [17,18], in which Sn weakens the bonding strength of the alkenes on the alloy surface, and promotes the desorption of alkene product easily compared to the pure Pt, however, it also reduces the rates of alkane dehydrogenation and its C–C bond cleavage

* Corresponding authors at: State Key Laboratory of Clean and Efficient Coal Utilization, Taiyuan University of Technology, Taiyuan 030024, Shanxi, PR China.
E-mail addresses: wangbaojun@tyut.edu.cn, wbj@tyut.edu.cn (B. Wang), zhangriguang@tyut.edu.cn (R. Zhang).

https://doi.org/10.1016/j.fuel.2021.121641
Received 21 April 2021; Received in revised form 25 July 2021; Accepted 1 August 2021
Available online 7 August 2021
0016-2361/© 2021 Elsevier Ltd. All rights reserved.

[19–21].

Above results show that in alkane dehydrogenation to alkene, the preference between alkene desorption and its dehydrogenation is the selectivity-determining step, increasing alkene selectivity by weakening alkene interaction with the catalyst surface will accompany activity decreasing due to the rate reduction of the dehydrogenation and C–C bond cleavage of the alkane. Thus, to achieve excellent activity and selectivity in ethane (C_2H_6) dehydrogenation to ethylene (C_2H_4), developing catalysts should focus on two key factors: one is to balance the activity between the dehydrogenation and C–C bond cleavage in the process of C_2H_6 dehydrogenation to C_2H_4, the other is to balance the competition between C_2H_4 desorption and its dehydrogenation/C–C bond cleavage.

In the recent ten years, Kyriakou *et al.* [22] firstly established the single-atom alloy (SAA) materials as a class of catalysts in 2012 and aroused widespread interest. SAA catalysts are usually composed of the inert metal substrate and active metal atoms dispersed on the inert metal surface, only 1% of active metal atom is isolated within the surface of inert metal host [23–25], which significantly improved the reactivity and kept the excellent selectivity of the host metal for numerous catalytic reactions [26–29]. This strategy facilitates the selective activation of the adsorbed species on the surface through the atomically dispersed active sites, whereas the reaction rate on the pure noble metal was limited. For example, the final C–H bond dissociation of methane leading to coke formation can be significantly inhibited on a series of Pd-, Pt-, Rh- and Ni-doped Cu SAA catalysts [30]; the same things also occur on the Ni-, Pd-, Pt- and Rh-doped Cu, Ag and Au SAA catalysts [31]. The Ir-, Pd-, Pt-, and Rh-doped Au, Ag and Cu SAA catalysts can selectively activate the C_α–H bond of ethanol in its partial oxidation to reduce the barrier of C–H bond cleavage [32]. For the alkane dehydrogenation, Pd-doped Cu SAA catalyst increases the activity of propane dehydrogenation besides propylene dehydrogenation, and propylene desorption takes precedence over side reactions, showing ideal propylene selectivity [33]. Butane dehydrogenation to butene on the Pt-doped Cu SAA catalyst exhibited moderate activity for C–H bond cleavage between the pure Pt and Cu, and prevents complete dehydrogenation [28]. The limitation of the scaling relationship of Pt alloy usually leads to an increase in the selectivity of propene, while the inherent activity of propane dehydrogenation is inhibited [8]. Further, propane conversion to propene on the Pt-doped Cu SAAs achieved 90% propene selectivity at 520 °C, and the theoretical calculation verifies that the coking was obviously reduced [34]. The isolated Pt atoms on the Pt-doped Cu SAAs facilitate the activation of ethyl in C_2H_6 dehydrogenation, while avoiding the C–C bond cleavage leading to the coking on Pt [35].

As mentioned above, SAA catalysts have become potential to provide excellent activity, selectivity, and stability toward the C–H bond activation and the selective dehydrogenation of alkanes, especially, propane and methane. However, to date, few studies were implemented to reveal the mechanism and catalytic performance of C_2H_6 dehydrogenation on the SAA catalysts, and the activity and selectivity on the SAA catalyst still remain elusive. Meanwhile, only a few of SAA materials have been synthesized, moreover, the conventional trial and error methods were employed to discover the newly-efficient catalytic materials, though this is both costly and time-consuming. Thus, the potential metallic combinations to best catalyze C_2H_6 dehydrogenation still keep unclear, and the catalyst screening of metal–metal combinations in the SAA catalysts with better activity and selectivity toward C_2H_6 dehydrogenation remain nontrivial tasks. Hopefully, with the rapid advances of parallel computation technique, the extensive screening of materials for chemical properties has been well realized using DFT calculations [36–38], which could provide fundamental insight into the properties and the catalyst function toward C_2H_6 dehydrogenation and realize the catalyst screening.

To shed light on above issue, this study is designed to carry out a widespread catalyst screening in C_2H_6 dehydrogenation using both density functional theory (DFT) and microkinetic modeling calculations, aiming at elucidating the fundamental catalytic properties of fifteen types of SAA catalysts including the single-atom Co, Ir, Ni, Pd and Pt doped-Cu, Ag and Au catalysts. Meanwhile, the structure-performance relationship of SAA catalyst was revealed by the analysis of electronic properties. Further, the dual descriptors were proposed to judge the catalytic activity and selectivity of C_2H_6 dehydrogenation. This work will ultimately be expected to aid the design and discovery of SAA catalysts with high-performance in alkane dehydrogenation, serving as a guide to experimentalists and theoreticians alike.

2. Computational methods and models

2.1. Methods

All DFT calculations were implemented using the Vienna *ab initio* simulation package (VASP) [39]. The electronic exchange and correlation were described using the generalized gradient approximation method with the Perdew-Burke-Ernzerhof functional (GGA-PBE) [40]. Core electrons were treated within the projector-augmented wave (PAW) framework, and the cut-off energy of the plane-wave basis was set as 400 eV [41,42]. The convergence criteria for the residual force on each atom fell below 0.02 eV·Å^{-1}, and the total energy difference during structure optimization was less than 10^{-5} eV. The Brillouin zone was sampled using a Monkhorst–Pack mesh *k*-point, which is the (5 × 5 × 1) mesh for the Cu- and Ag-based SAAs, the (4 × 4 × 1) mesh for Au-based SAAs. For the pure metal slab and Pt_3Sn alloy surfaces, that is the (3 × 3 × 1) mesh for Pt, the (4 × 4 × 1) mesh for Cr, the (5 × 5 × 1) mesh for Pd and (3 × 3 × 1) mesh for Pt_3Sn [43]. Dispersion correction was modeled using DFT-D3 method [44]. The climbing image-nudged elastic band (CI-NEB) method was employed to acquire an approximate minimum reaction energy path [45,46]. The transition state was located by the dimer method until to energy convergence of 0.05 eV·Å^{-1}. All transition states were verified by vibrational frequency analysis [47].

The zero-point energy (ZPE) and free energy correction of the gas phase and adsorbed molecules were carried out through the VASPKIT software package [48] at the typical experimental conditions of C_2H_6 dehydrogenation (873.15 K and 1 atm) [49–51]. The electronic properties including the projected density of states, Bader charge, charge density difference, and projected Crystal Orbital Hamilton Population (pCOHP) were analyzed. All details were presented in the Supplementary Material.

2.2. Models

For fifteen types of SAA catalysts including the single-atom Co, Ir, Ni, Pd and Pt doped-Cu, Ag and Au catalysts, the SAA catalyst models were constructed by replacing a surface atom of the substrate with a doping metal atom, as shown in Fig. 1. The substrate materials of Cu(1 1 1), Ag (1 1 1) and Au(1 1 1) were modeled with the four-layer $p(3 \times 3)$ supercell. For the metal slab surfaces, Pt(1 1 1) was modeled with the five-layer $p(3 \times 3)$, Cr(1 1 0) and Pd(1 1 1) were modeled by the four-layer $p(3 \times 2)$ and $p(3 \times 3)$, respectively. For Pt_3Sn(1 1 1) surfaces, the model is to use a four-layer $p(4 \times 4)$. A vacuum of 15 Å was employed to eliminate the mutual interaction between the slabs. During the optimization, the bottom one layer of the catalyst slab was frozen, while the other layers were relaxed.

3. Results and discussions

Previous works [49,52,53] have investigated the full reaction network of ethane dehydrogenation on the Pt, Pt-M alloy and other close-packed metal catalysts, indicating that the isomerization reaction of C_2 species (CH_2CH_2 and CH_3CH, CH_3C and CH_2CH, and CHCH and CH_2C) in C_2H_6 dehydrogenation is difficult to occur, which is excluded in this study, other reactions are all considered. As a result, the considered elementary reactions in the process of C_2H_6 dehydrogenation

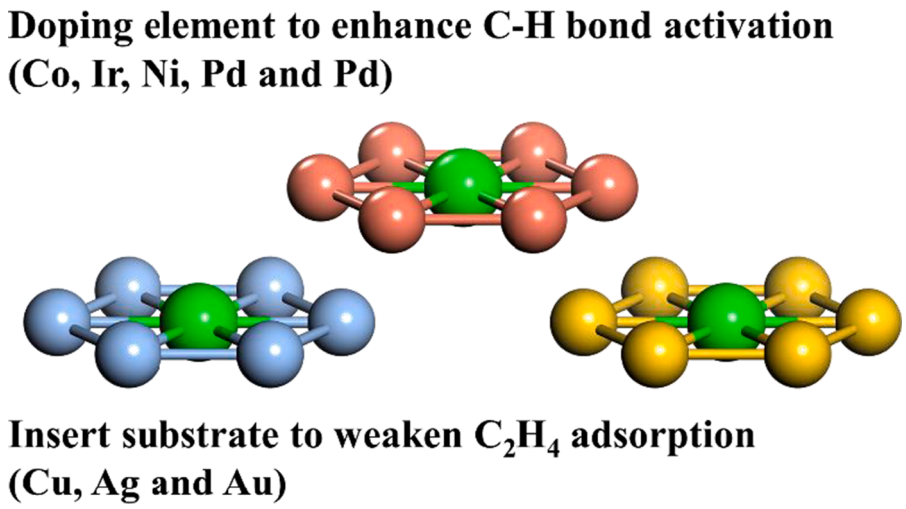

Fig. 1. The models of SAA catalysts by replacing a surface atom of the substrate with a doping metal atom. Green balls represent the single-atom element (Co, Ir, Ni, Pd and Pt), the orange, blue and yellow balls represent the inert elements (Cu, Ag and Au) of the substrate, respectively. (For interpretation of the references to colour in this figure legend, the reader is referred to the web version of this article.)

in this study are presented in Fig. 2. Firstly, C_2H_6 molecule is adsorbed onto the catalyst surface, the first dehydrogenation process has two steps: the dehydrogenation to C_2H_5* and the C–C bond cleavage to two CH_3*. Then, starting from the intermediate C_2H_5*, the second dehydrogenation process includes three steps: the dehydrogenation to either $CHCH_3$* or C_2H_4*, and the C–C bond cleavage to CH_2*+CH_3*. Further, C_2H_4* desorption process involves three steps: C_2H_4* desorption to produce gas phase C_2H_4, the dehydrogenation to C_2H_3*, and the C–C bond cleavage to two CH_2*.

It is noted that the production of $CHCH_3$*, C_2H_3* and CH_x*(x = 1–3) will reduce the productivity and selectivity of C_2H_4*. Previous work [52,54,55] showed that both $CHCH_3$* and C_2H_3* are the precursors of coke formation in C_2H_6 dehydrogenation, their dehydrogenation ($CHCH_3$*→$CHCH_2$*/CCH_3*→$CHCH$*/CCH_2*→CCH*→CC*) or the C–C bond cleavage ($CHCH_x$*→CH*+CH_x*(x = 1–3), C_2H_3*→CH*+CH_2* and CCH_x*→C*+CH_x*), and the dehydrogenation of CH_x*(x = 1–3) will result in coke deposition. Thus, in the process of C_2H_6 dehydrogenation, both the C–C bond cleavage of C_2 species to CH_x*(x = 1–3) and the production of $CHCH_3$ and C_2H_3* precursors are expected to be suppressed.

Based on above analysis, aiming at identifying whether the gas phase C_2H_4 prefers to be produced in C_2H_6 dehydrogenation, the first is to obtain the preference between C_2H_4* desorption and its dehydrogenation to C_2H_3*/its C–C bond cleavage. Secondly, when C_2H_4* desorption is favored, starting from C_2H_5*, judging whether its dehydrogenation to C_2H_4* is also favored compared to its dehydrogenation to $CHCH_3$* and its C–C bond cleavage. Thirdly, when C_2H_4* formation is favored, evaluating whether C_2H_6* dehydrogenation to C_2H_5* is still favored compared to its C–C bond cleavage. Based on three aspects of analysis, the catalysts with good C_2H_4* selectivity can be screened out. All energy data of the elementary reactions are listed in Table 1.

3.1. The reactions involving in the desorption process of C_2H_4*

In the desorption process of C_2H_4*, starting from C_2H_4*, Fig. 3 presents C_2H_4* desorption energy, the activation free energy of C_2H_4* dehydrogenation to C_2H_3*, and the reaction free energy of C–C bond cleavage on the Cu-, Au-, Ag-based SAA catalysts (see details in Figs. S1 ~ S3). When C_2H_4* desorption energy becomes negative, it means that C_2H_4* desorption is spontaneous process, and it is exothermic. Previous studies [49,56,57] showed that the more negative the value of C_2H_4* desorption energy is, the easier C_2H_4* desorption is. As shown in Fig. 3, our results show that C_2H_4* desorption to gas phase C_2H_4 is much easier in kinetics than its dehydrogenation and C–C bond cleavage on all considered Cu-, Au-, Ag-based SAA catalysts. In a word, these catalysts at the typical experimental temperature 873.15 K facilitate C_2H_4* desorption to produce gas phase C_2H_4. In addition, Sun *et al.* [34] also found that the Pt doped-Cu SAA catalyst facilitates propylene desorption and inhibit its further dehydrogenation. Cao *et al.* [33] studied the activity of Pd doped-Cu SAA catalyst for propane dehydrogenation, suggesting that propylene desorption is much easier than its dehydrogenation and C–C bond cleavage.

On the other hand, for C_2H_4* dehydrogenation and its C–C bond cleavage, among all considered catalysts, only IrAg and IrAu catalysts

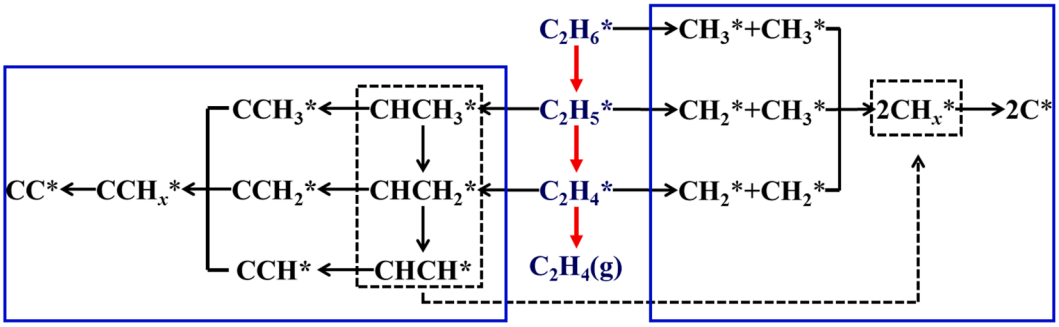

Fig. 2. The reaction network of C_2H_6 dehydrogenation including the processes of C_2H_6 dehydrogenation to gas phase C_2H_4 (solid red arrows), coking formation by deep dehydrogenation path (left blue box) and the C–C bond cleavage path (dotted box and right blue box). x = 1–3, * and (g) corresponds to the adsorbed and gaseous states, respectively. (For interpretation of the references to colour in this figure legend, the reader is referred to the web version of this article.)

Table 1
Activation free energy (G_a) and reaction free energy (ΔG) of the elementary reactions involving in C_2H_6 dehydrogenation on all considered catalysts at 873.15 K and 1 atm.

Reactions		$G_a(\Delta G)$(kJ·mol^{-1})				
		Cu-based SAA catalysts				
		CoCu	**IrCu**	**NiCu**	**PdCu**	**PtCu**
R1	C_2H_6*→C_2H_5*+H*	49.5(16.5)	44.0(9.2)	72.8(25.9)	89.3(54.6)	73.3(35.4)
R2	C_2H_6*→CH_3*+CH_3*	156.4(52.8)	—	167.6(59.9)	202.2(47.0)	220.2(21.5)
R3	C_2H_5*→CH_2*+CH_3*	113.7(20.6)	186.5(95.3)	154.7(130.4)	135.3(81.2)	158.9(68.7)
R4	C_2H_5*→C_2H_4*+H*	3.9(-54.2)	70.7(52.5)	13.9(-5.6)	43.8(-6.6)	74.1(41.9)
R5	C_2H_5*→$CHCH_3$*+H*	14.6(-27.6)	61.9(20.0)	51.2(28.7)	92.9(50.5)	95.7(59.2)
R6	C_2H_4*→CH_2*+CH_2*	(107.1)	(122.4)	(127.8)	(196.7)	(160.0)
R7	C_2H_4*→C_2H_3*+H*	66.7(64.9)	75.1(19.1)	71.3(42.2)	110.7(58.3)	90.2(46.6)
R8	C_2H_4*→C_2H_4(g)	(-3.4)	(-5.7)	(-26.4)	(-53.1)	(-46.8)
		Ag-based SAA catalysts				
		CoAg	**IrAg**	**NiAg**	**PdAg**	**PtAg**
R1	C_2H_6*→C_2H_5*+H*	75.0(50.0)	27.9(-5.8)	75.0(63.6)	113.1(100.9)	70.6(43.7)
R2	C_2H_6*→CH_3*+CH_3*	—	143.2(94.5)	167.2(97.0)	241.4(131.6)	236.1(82.8)
R3	C_2H_5*→CH_2*+CH_3*	180.0(131.2)	190.6(109.7)	193.7(129.5)	184.0(162.1)	218.6(163.1)
R4	C_2H_5*→C_2H_4*+H*	19.3(-21.6)	48.5(-14.8)	20.8(4.1)	67.9(37.5)	92.5(64.6)
R5	C_2H_5*→$CHCH_3$*+H*	10.5(5.0)	51.3(6.3)	63.3(61.3)	113.1(98.7)	109.0(84.2)
R6	C_2H_4*→CH_2*+CH_2*	(120.1)	(134.8)	(170.0)	(240.9)	(190.0)
R7	C_2H_4*→C_2H_3*+H*	60.9(42.4)	148.0(89.7)	65.3(63.8)	93.5(81.7)	70.3(61.1)
R8	C_2H_4*→C_2H_4(g)	(-20.9)	(-3.7)	(-45.8)	(-69.3)	(-64.2)
		Au-based SAA catalysts				
		CoAu	**IrAu**	**NiAu**	**PdAu**	**PtAu**
R1	C_2H_6*→C_2H_5*+H*	56.6(43.0)	42.2(3.8)	77.7(75.3)	121.4(94.5)	60.0(35.5)
R2	C_2H_6*→CH_3*+CH_3*	—	—	281.5(109.1)	278.4(141.6)	—
R3	C_2H_5*→CH_2*+CH_3*	206.3(86.9)	205.2(107.0)	198.0(117.0)	187.6(141.0)	220.6(135.8)
R4	C_2H_5*→C_2H_4*+H*	66.0(19.6)	61.4(0.7)	43.5(32.4)	46.7(31.3)	116.2(36.6)
R5	C_2H_5*→$CHCH_3$*+H*	27.5(18.2)	46.2(18.6)	72.7(64.4)	116.2(86.6)	108.1(75.7)
R6	C_2H_4*→CH_2*+CH_2*	(131.0)	(127.2)	(159.4)	(212.7)	(162.0)
R7	C_2H_4*→C_2H_3*+H*	113.2(75.8)	139.6(109.7)	86.3(81.9)	97.0(84.0)	87.6(65.9)
R8	C_2H_4*→C_2H_4(g)	(-27.9)	(-9.6)	(-56.1)	(-65.6)	(-57.7)
		The pure metal and alloy catalysts				
		Pd	**Pt**	**Cr**	**Pt_3Sn**	**Cu**
R1	C_2H_6*→C_2H_5*+H*	58.2(6.8)	49.8(-30.0)	85.5(-77.8)	58.2(-0.1)	132.7(69.6)
R2	C_2H_6*→CH_3*+CH_3*	245.2(80.6)	251.1(-10.3)	53.4(-116.9)	259.6(45.4)	295.4(88.2)
R3	C_2H_5*→CH_2*+CH_3*	192.4(67.7)	168.1(-6.5)	111.8(-72.5)	188.8(52.4)	130.5(73.2)
R4	C_2H_5*→C_2H_4*+H*	42.0(-24.5)	60.4(-24.4)	18.6(-58.0)	66.0(28.0)	41.0(0.4)
R5	C_2H_5*→$CHCH_3$*+H*	79.4(-12.7)	76.1(-2.5)	46.9(-38.3)	45.9(-1.3)	82.0(44.6)
R6	C_2H_4*→CH_2*+CH_2*	184.1(131.9)	197.6(73.9)	71.3(-38.2)	245.9(134.4)	(151.9)
R7	C_2H_4*→C_2H_3*+H*	104.8(22.1)	66.6(-1.5)	33.0(-58.3)	75.2(30.2)	119.6(49.1)
R8	C_2H_4*→C_2H_4(g)	(1.3)	(18.0)	(52.1)	(-18.7)	(-68.7)
		Ag	**Au**			
R1	C_2H_6*→C_2H_5*+H*	196.1(162.5)	166.7(115.9)			
R2	C_2H_6*→CH_3*+CH_3*	333.6(187.1)	294.5(141.5)			
R3	C_2H_5*→CH_2*+CH_3*	224.5(163.6)	234.8(166.0)			
R4	C_2H_5*→C_2H_4*+H*	74.8(15.1)	109.1(56.2)			
R5	C_2H_5*→$CHCH_3$*+H*	158.8(134.8)	209.1(129.0)			
R6	C_2H_4*→CH_2*+CH_2*	(309.2)	(395.0)			
R7	C_2H_4*→C_2H_3*+H*	165.2(112.5)	134.3(89.4)			
R8	C_2H_4*→C_2H_4(g)	(-98.5)	(-99.2)			

favored the C–C bond cleavage rather than its dehydrogenation, whereas other types of SAA catalysts favor its hydrogenation instead of its C–C bond cleavage, previous studies also support our results, for example, Nam *et al.* [55] found that the C–C bond cleavage of C_2H_4* is difficult compared to its desorption and dehydrogenation on the Pt(111) and Pt_3Sn(111). Saelee *et al.* [58] and Yang *et al.* [59] studied propane dehydrogenation on the Ni(111), Pt(111) and Pt(211), and the C–C bond cleavage of propylene is still hard compared to its dehydrogenation.

3.2. The reactions involving in the dehydrogenation process of C_2H_5*

As mentioned above, since C_2H_4* desorption is more favored on all considered SAA catalysts, starting from C_2H_5*, we further judge whether its dehydrogenation to C_2H_4* is also kinetically superior to its dehydrogenation to $CHCH_3$* and its C–C bond cleavage. Fig. 4 presents the activation free energy of C_2H_5* dehydrogenation to C_2H_4* and $CHCH_3$*, and its C–C bond cleavage on the Cu-, Au-, Ag-based SAA catalysts (see details in Figs. S1 ~ S3).

On the Cu-based SAA catalysts, see Fig. 4a, IrCu is kinetically favored for $CHCH_3$* formation compared to C_2H_4* formation and its C–C bond cleavage (61.9 *vs.* 70.7, 186.5 kJ·mol^{-1}); whereas the CoCu, NiCu, PdCu and PtCu catalysts prefer to produce C_2H_4* in kinetics compared to $CHCH_3$ formation and its C–C bond cleavage. Namely, IrCu cannot produce C_2H_4* in C_2H_5* dehydrogenation, while the CoCu, NiCu, PdCu and PtCu catalysts favor C_2H_4* formation, the activity order is CoCu > NiCu > PdCu > PtCu (3.9, 13.9, 43.8 and 74.1 kJ·mol^{-1}).

On the Ag-based SAA catalysts, see Fig. 4b, CoAg is kinetically favorable for $CHCH_3$* formation, while the IrAg, NiAg, PdAg and PtAg favored C_2H_4* formation, the activity is NiAg > IrAg > PdAg > PtAg (20.8, 48.5, 67.9 and 92.5 kJ·mol^{-1}). On the Au-based SAA catalysts, see Fig. 4c, the CoAu, IrAu and PtAu are kinetically favorable for $CHCH_3$* formation, while both NiAu and PdAu catalysts favored C_2H_4* formation, the activity is NiAu > PdAu (43.5 and 46.7 kJ·mol^{-1}).

Above results show that ten types of SAA catalysts, including the CoCu, NiCu, PdCu, PtCu, IrAg, NiAg, PdAg, PtAg, NiAu and PdAu, favor

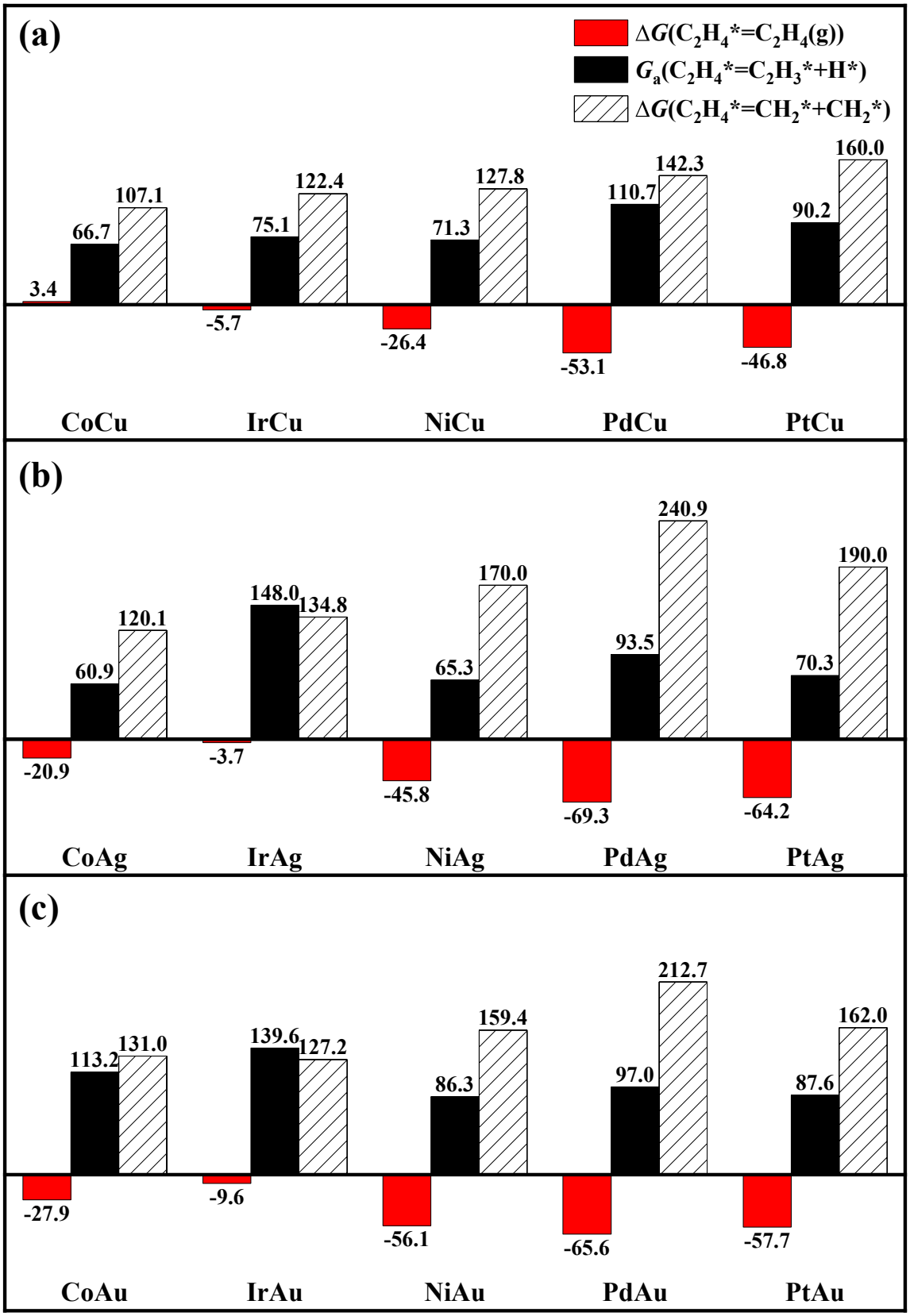

Fig. 3. The desorption free energy of C_2H_4*, the activation free energy of C_2H_4* dehydrogenation, and the reaction free energy of C–C bond cleavage for C_2H_4* on the (a) Cu-based, (b) Ag-based, and (c) Au-based SAA catalysts at 873.15 K and 1 atm.

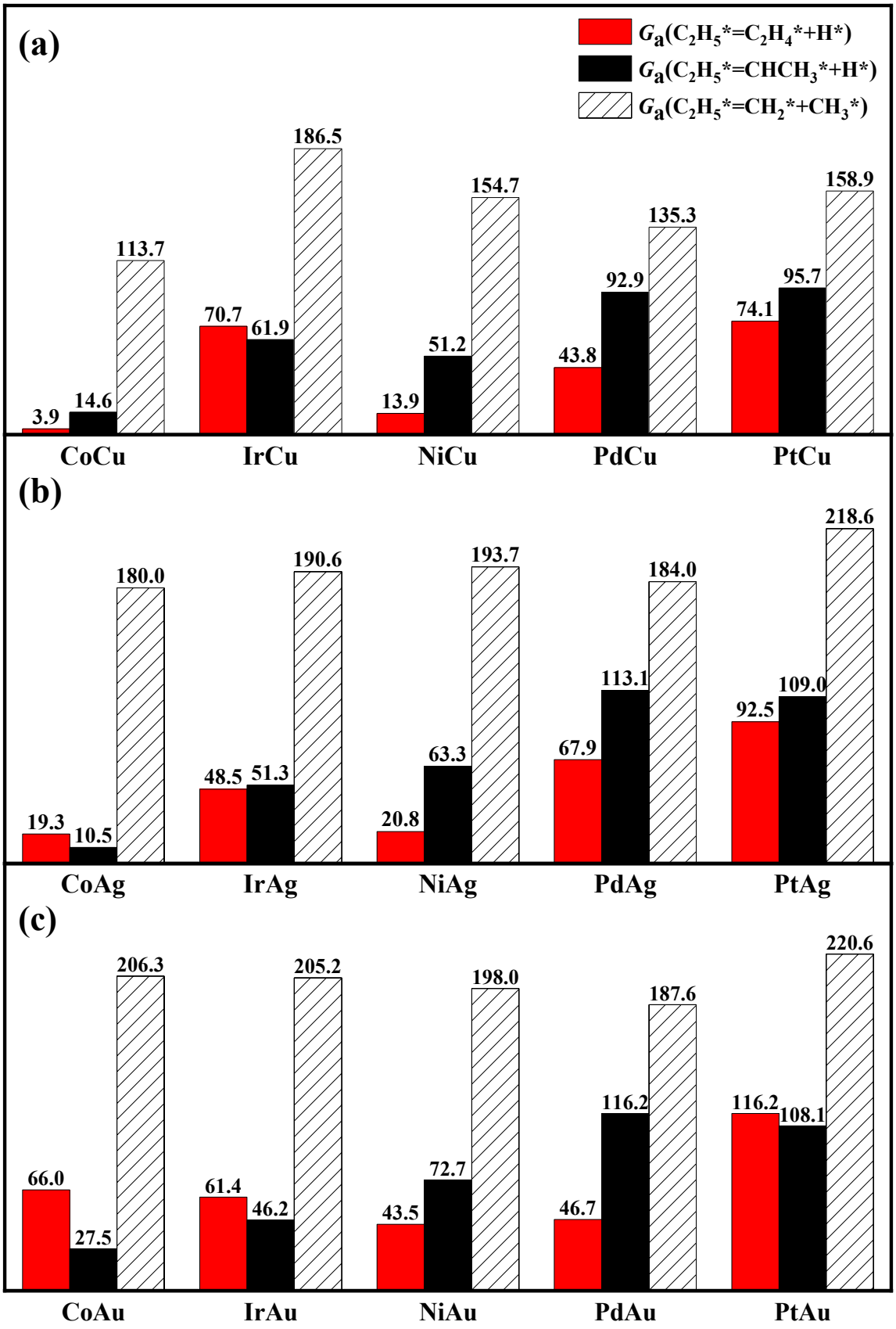

Fig. 4. The activation free energy of $C_2H_5^*$ dehydrogenation to $C_2H_4^*$ and $CHCH_3^*$, and its C–C bond cleavage to $CH_2^*+CH_3^*$ on the (a) Cu-based, (b) Ag-based, and (c) Au-based SAA catalysts at 873.15 K and 1 atm.

C_2H_4* formation, while five types of SAA catalysts, including the IrCu, CoAg, CoAu, IrAu and PtAu, prefer to $CHCH_3$* formation, which leads to carbon deposition and reduces C_2H_4* selectivity. Thus, these five types of SAA catalysts, IrCu, CoAg, CoAu, IrAu and PtAu, are unfavorable for C_2H_6 dehydrogenation to produce gas phase C_2H_4. In addition, C_2H_6 dehydrogenation on the Pt_3Sn and PtCu also shows that when $CHCH_3$* is easily formed in C_2H_5* dehydrogenation, C_2H_4 selectivity decreases [35,60].

3.3. The reactions involving in the dehydrogenation process of C_2H_6*

As mentioned above, since ten types of SAA catalysts, CoCu, NiCu, PdCu, PtCu, IrAg, NiAg, PdAg, PtAg, NiAu and PdAu, favored C_2H_5* dehydrogenation to produce C_2H_4*, the dehydrogenation process of C_2H_6* was further examined. Fig. 5 presents the activation free energies of C_2H_6 dehydrogenation to C_2H_5* and its C–C bond cleavage to two CH_3* on ten types of SAA catalysts (see details in Figs. S1 ~ S3).

On the Cu-based SAA catalysts, see Fig. 5, C_2H_6* dehydrogenation to C_2H_5* on the CoCu, NiCu, PdCu and PtCu (49.5, 72.8, 89.3, 73.3 kJ·mol^{-1}) is more preferred in kinetics compared to its C–C bond cleavage (156.4, 167.6, 202.2, 220.2 kJ·mol^{-1}), namely, these four types of catalysts are in favor of C_2H_6* dehydrogenation rather than its C–C bond cleavage, and C_2H_5* is the dominant intermediate. Meanwhile, the activity of C_2H_6* dehydrogenation to C_2H_5* is CoCu > NiCu > PtCu > PdCu.

On the Ag-based SAA catalysts, C_2H_6* dehydrogenation to C_2H_5* on the IrAg, NiAg, PdAg and PtAg (27.9, 75.0, 113.1, 70.6 kJ·mol^{-1}) is also preferred kinetically than its C–C bond cleavage (143.2, 167.2, 241.4, 236.1 kJ·mol^{-1}); the activity is IrAg > PtAg > NiAg > PdAg. On the Au-based SAA catalysts, C_2H_6* dehydrogenation to C_2H_5* on the NiAu and PdAu (77.7 and 121.4 kJ·mol^{-1}) is more favored than its C–C bond cleavage (281.5, 278.4 kJ·mol^{-1}); the activity is NiAu > PdAu.

Above results show that C_2H_6* dehydrogenation to C_2H_5* is kinetically superior to its C–C bond cleavage on ten types of Cu-, Au-, Ag-based SAA catalysts. In addition, Hansen *et al.* [49] and Nam *et al.* [55] theoretically performed C_2H_6 dehydrogenation on Pt(1 1 1) and Pt_3Sn (1 1 1), the kinetics results show that the C–H bond activation of C_2H_6* is much easier than its C–C bond cleavage.

3.4. General discussions

Based on above three aspects of analysis (C_2H_4* desorption, C_2H_5* dehydrogenation and C_2H_6* dehydrogenation), ten types of Cu-, Au-, Ag-based SAA catalysts, CoCu, NiCu, PdCu, PtCu, IrAg, NiAg, PdAg, PtAg, NiAu and PdAu, are screened out to exhibit better selectivity toward gas phase C_2H_4.

3.4.1. The activity analysis of C2H6 dehydrogenation to produce gas phase C_2H_4

Previous studies [8,60,61] have shown that the first or second dehydrogenation of light alkanes is identified as the rate-determining step, meanwhile, our results also proved that C_2H_4* desorption is not the rate-determining step on the screened ten types of Cu-, Au-, Ag-based SAA catalysts. Thus, the activation free energy for the dehydrogenation step of C_2H_6* and C_2H_5* could reflect the catalytic activity of C_2H_6 dehydrogenation on the catalysts. Here, the activity analysis for the screened ten types of SAA catalysts, including the CoCu, NiCu, PdCu, PtCu, IrAg, NiAg, PdAg, PtAg, NiAu and PdAu, were carried out.

As presented in Fig. 6a, the activation free energy of C_2H_6* dehydrogenation is higher than that of C_2H_5* dehydrogenation on the CoCu, NiCu, PdCu, NiAg, PdAg, NiAu and PdAu catalysts, suggesting that C_2H_6* first dehydrogenation is the rate-determining step on these catalysts; whereas the dehydrogenation of C_2H_5* is the rate-determining step on the PtCu, IrAg and PtAg catalysts.

As illustrated in Fig. 6b, the overall barrier of C_2H_6* dehydrogenation to gas phase C_2H_4 on ten types of SAA catalysts showed that the activity of C_2H_6* dehydrogenation to C_2H_4* is in sequence of IrAg > CoCu > NiCu > PtCu > NiAg > NiAu > PdCu > PtAg > PdAg > PdAu (48.5, 49.5, 72.8, 74.1, 75.0, 77.7, 89.3, 92.5, 113.1 and 121.4 kJ·mol^{-1}), thus, the IrAg, CoCu and NiCu have higher activity, and the PtAg, PdAg and PdAu have lower activity for C_2H_6* dehydrogenation to gas phase C_2H_4.

On the other hand, previous work has shown that the adsorption energy of adsorbed species involved in the targeted reactions is often related to the barriers of this targeted reaction [62]. For example, Zhao *et al.* [63] showed that the adsorption energy of C_2H_2 is positively correlated with the barrier of C_2H_4* formation in C_2H_2 selective

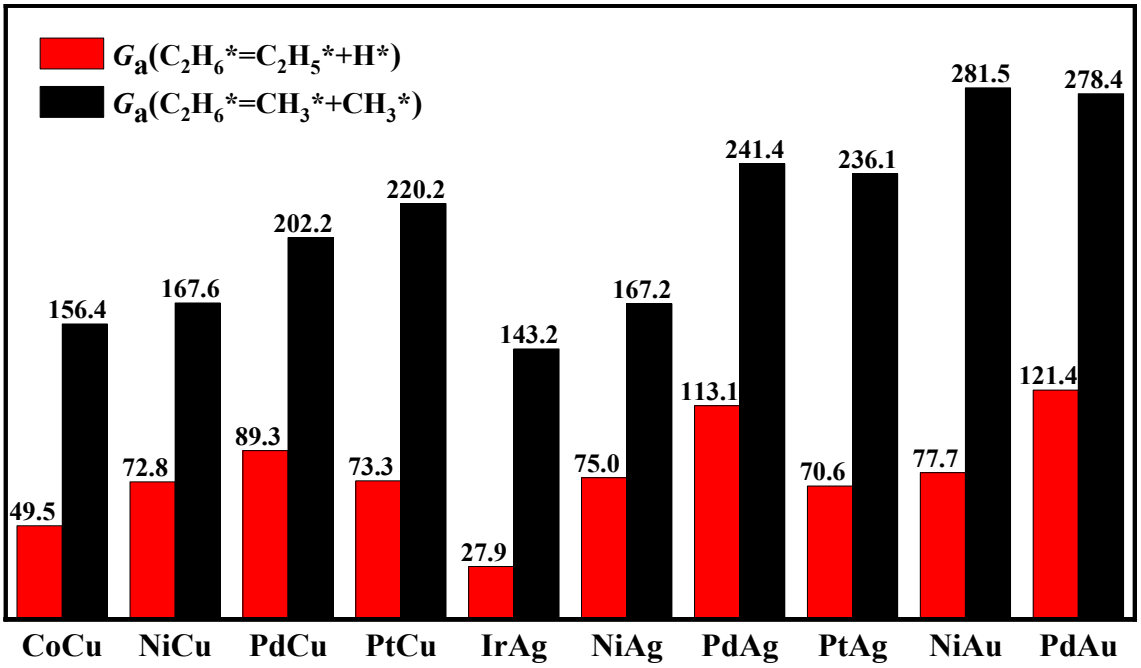

Fig. 5. The activation free energies of C_2H_6* dehydrogenation to C_2H_5* and its C–C bond cleavage to CH_3*+CH_3* on the Cu-, Au-, Ag-based SAA catalysts at 873.15 K and 1 atm.

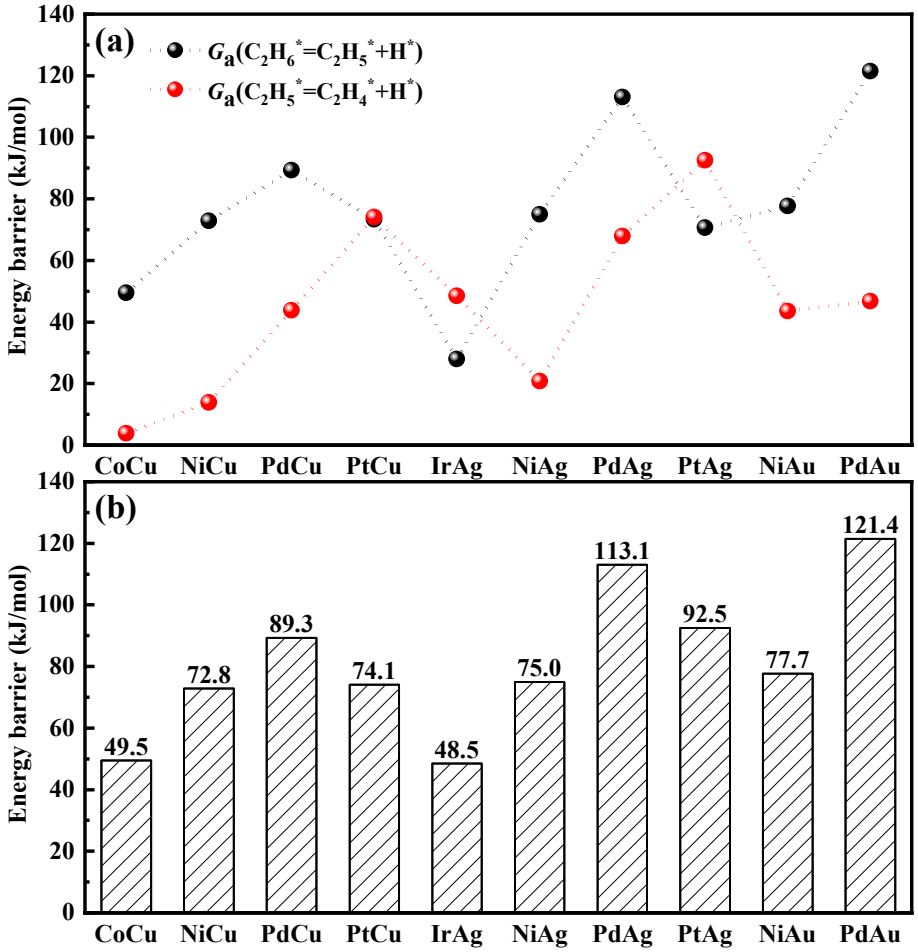

Fig. 6. (a) The activation free energy for the dehydrogenation steps of C_2H_6* and C_2H_5*, and (b) the overall barrier of C_2H_6* dehydrogenation to gas phase C_2H_4 on ten types of SAA catalysts at 873.15 K and 1 atm.

hydrogenation on the transition metals. The theoretical studies by Studt *et al.* [64] found the turnover frequency of methanol and the adsorption energy of O* on different NiGa alloy surfaces could plotted as a volcano curve for the activity of CO_2 hydrogenation to methanol. Thus, as shown in Fig. 7a, the relationship between C_2H_4* desorption energy and the overall barrier of C_2H_6* dehydrogenation to gas phase C_2H_4 was analyzed, indicating that with the decreasing of C_2H_4* desorption energy, the overall barrier of gas phase C_2H_4 production increases, and therefore the activity of C_2H_6* dehydrogenation to gas phase C_2H_4 decreases, namely, the easier the desorption of C_2H_4* is, the lower the activity of C_2H_6* dehydrogenation to gas phase C_2H_4 is, which is consistent with the reportedly experimental results [8,34,35,49]. Thus, it is believed that C_2H_4* desorption energy can be used to evaluate the activity of C_2H_6* dehydrogenation to gas phase C_2H_4.

Further, when the transition metals are doped into the inert metals, the *d*-band center will move, and the change of the binding energies for the adsorbed species could be attributed to the changes of electronic interaction based on the ligand effect [65,66]. The projected density of state (*p*DOS) for the pure metals Cu, Ag, Au, and fifteen types of Cu-, Ag- and Au-based SAA catalysts (see Fig. S6) showed that *d*-band center of surface atoms is limited by the substrate metal Cu, Ag and Au with *d*-band center values of −2.23, −3.98 and −3.24 eV, respectively. Meanwhile, previous studies [67–69] also confirmed that the *d*-band center was closely related to the desorption energy of adsorbed species on the transition metals. As shown in Fig. 7b, when the active metals Ir, Ni, Pt and Pd is doped into the substrate metal Cu, compare to the pure metal Cu, the *d*-band centers of PdCu, PtCu, NiCu and IrCu are gradually close to the Fermi level, correspondingly, C_2H_4* desorption energy gradually increases. The same things also occur on the substrate metals Ag and Au. The same thing also occurred for CH_4 dehydrogenation on various Cu-based SAA catalysts [65].

3.4.2. *The selectivity trend of C_2H_6 dehydrogenation to gas phase C_2H_4*

As mentioned above, among two dehydrogenation steps and one desorption step involving in C_2H_6* dehydrogenation to gas phase C_2H_4, C_2H_6* dehydrogenation to C_2H_5* on ten types of SAA catalysts is much easier in kinetics than its C–C bond cleavage; similarly, C_2H_4* desorption is also much easier in kinetics than its dehydrogenation and C–C bond cleavage. Namely, C_2H_6* first dehydrogenation step and C_2H_4* desorption step hardly affect the selectivity of gas phase C_2H_4 in C_2H_6 dehydrogenation. Thus, the key factor that affects the selectivity of gas phase C_2H_4 dominantly focus on C_2H_5* dehydrogenation step, however, the C–C bond cleavage of C_2H_5* is very difficult in kinetics, so the selectivity of gas phase C_2H_4 is mainly controlled by C_2H_5* dehydrogenation to produce C_2H_4* and $CHCH_3$*.

Previous work found that the energy barrier difference between two steps that starting from the same initial reactant could be used as the simplest descriptor to quantitatively evaluate the selectivity [34,55], thus, starting from C_2H_5* dehydrogenation, the selectivity of gas phase C_2H_4 on ten types of SAA catalysts follows the order of PdAu > PdCu > PdAg > NiAg > NiCu > NiAu > PtCu > PtAg > CoCu > IrAg (69.5, 49.1, 45.2, 42.5, 37.3, 29.2, 21.6, 16.5, 10.7 and 2.8 kJ·mol^{-1}). Here, PdAu, PdCu, PdAg, NiAg, NiCu and NiAu are considered to exhibit better C_2H_4* selectivity, and IrAg has a poor C_2H_4* selectivity.

Similar to the activity analysis, as shown in Fig. 8a, the relationship of C_2H_5* adsorption energy with the energy barrier difference between

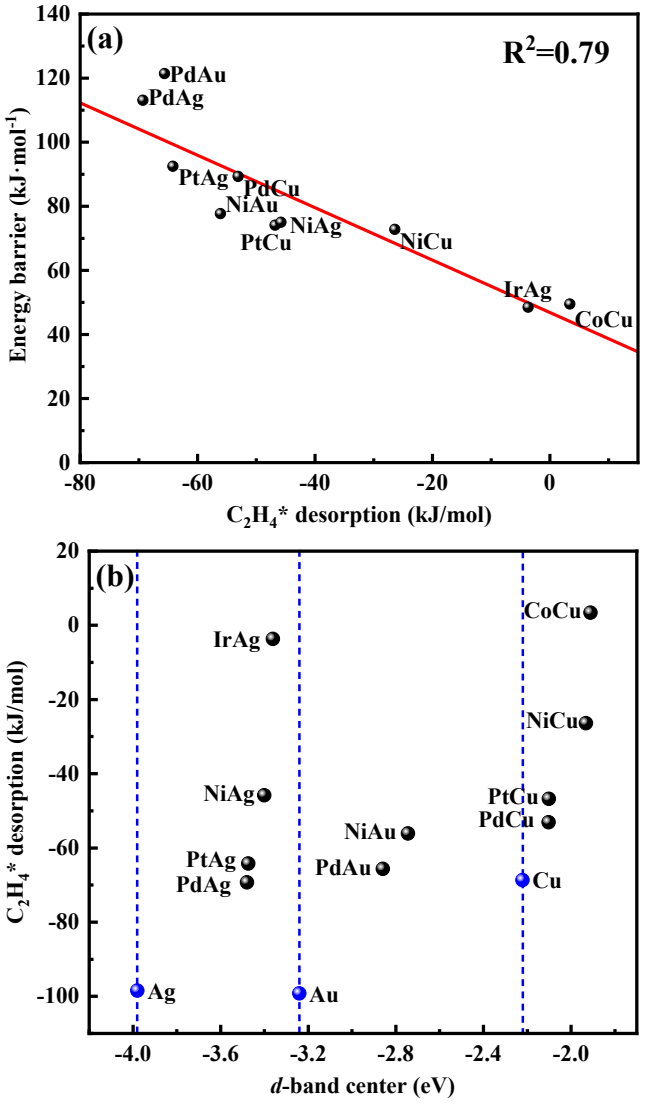

Fig. 7. Relationship of (a) C_2H_4* desorption free energy with the overall barrier of C_2H_6* dehydrogenation to gas phase C_2H_4, (b) the *d*-band center of surface atoms with C_2H_4* desorption free energy on thirteen types of pure metal Cu, Ag, Au and SAA catalysts at 873.15 K and 1 atm.

C_2H_5* dehydrogenation to $CHCH_3$* and C_2H_4* show that with the decreasing of C_2H_5* adsorption energy, the energy barrier difference increases, namely, the selectivity of C_2H_4* increases. Thus, C_2H_5* adsorption energy on the SAA catalysts can reflect C_2H_4* selectivity, the weaker the adsorption energy of C_2H_5* is, the higher the selectivity of C_2H_4* is.

On the other hand, when C_2H_5* was adsorbed on the Cu-, Ag-, and Au-based SAA catalysts, the interaction between C_2H_5* and the substrate is affected by the strain effect or ligand effect, leading to the influence on the adsorption energy of C_2H_5* [23,70]. pCOHP analysis for C_2H_5* adsorbed on the SAA catalysts surface was carried out, which can present the electron interaction strength of bonding and anti-bonding orbitals between the doping metal elements and the bonding state of C atom linked with the metals (see Fig. S7). The bonding state and anti-bonding state correspond to positive and negative values of vertical coordinates, respectively [71,72]. The anti-bonding states above the Fermi level of all SAA catalysts in the pCOHP diagrams are very weak, indicating that the adsorption strength of C_2H_5* is mainly determined by the bonding orbital. We integrated the bonding state above the Fermi level, and considered the correlation between the pCOHP integral and

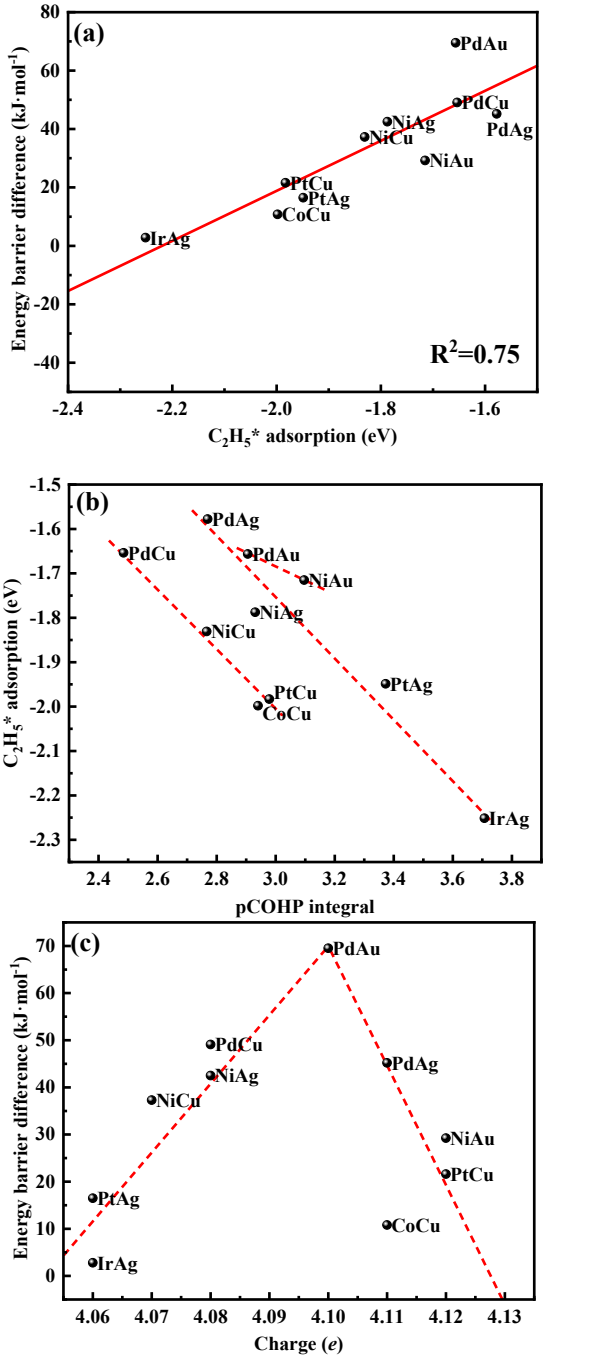

Fig. 8. Relationship of (a) the adsorption energy of C_2H_5* with the energy barrier difference of C_2H_5* dehydrogenation to $CHCH_3$* and C_2H_4*, (b) the pCOHP integral with the adsorption energy of C_2H_5*, (c) the charge of C_β in C_2H_5* with the energy barrier difference of C_2H_5* dehydrogenation to $CHCH_3$* and C_2H_4* on ten types of SAA catalysts.

C_2H_5* adsorption energy, as presented in Fig. 8b, pCOHP integral values increase, C_2H_5* adsorption energy of increase on all considered Cu-, Ag-, and Au-based SAA catalysts, indicating that the adsorption energy of C_2H_5* has a positive correlation with the bonding strength; similarly, the studies by Niu *et al.* [73] for oxygen reduction reaction on TM/g-C_3N_4 catalysts also showed that the pCOHP integral values between the 4*d* TM centers and the OH intermediate decrease, the adsorption energy of OH intermediate increases.

Further, to reveal the influence of C_2H_5* adsorption energy on C_2H_4* selectivity, the Bader charge of C_2H_5* adsorbed on the SAA catalysts was

analyzed (see Table S2), in which the C atom of C_2H_5* that is in the bonding state with the metal is defined as C_α, and the second C atom of C_2H_5* is defined as C_β. During the dehydrogenation process of C_2H_5*, the ability of C_β–H bond cleavage affects the selectivity of C_2H_4*. As shown in Fig. 8c, the energy barrier difference between C_2H_5* dehydrogenation to $CHCH_3$* and its dehydrogenation to C_2H_4* has the close relationship with the charge of C_β, that is, the relationship between the selectivity of C_2H_4* and the charge of C_β presents a volcanic curve, when the charge of C_β gradually increased to 4.10 *e*, the selectivity of C_2H_4* reach the maximum on PdAu catalyst. Therefore, the moderate charge of C_β in C_2H_5* decreases the competition between C_2H_5* dehydrogenation to C_2H_4* and its dehydrogenation to $CHCH_3$*, and enhance the selectivity of C_2H_4*.

3.5. Microkinetic modeling

To clearly illustrate the catalytic performance under the realistic reaction conditions, the selectivity and formation rate of C_2H_4* were analyzed using microkinetic modeling calculations (see details in the Supplementary Material).

As shown in Fig. 9a and Table S5, the relationship between C_2H_5* adsorption energy and C_2H_4* selectivity and formation rate showed that with the decreasing of C_2H_5* adsorption energy, C_2H_4* selectivity increases. Five types of IrCu, CoAg, CoAu, IrAu and PtAu catalysts exhibit poor C_2H_4* selectivity, however, among ten types of SAA catalysts, the PdAu, PdCu, NiCu, PdAg and NiAg catalysts showed better C_2H_4* selectivity, which is consistent with the selectivity trend results in Section 3.4.2. As shown in Fig. 9b and Table S5, the relationship between C_2H_4* desorption energy and C_2H_4* selectivity and formation rate showed that with the decreasing of C_2H_4* desorption energy, the

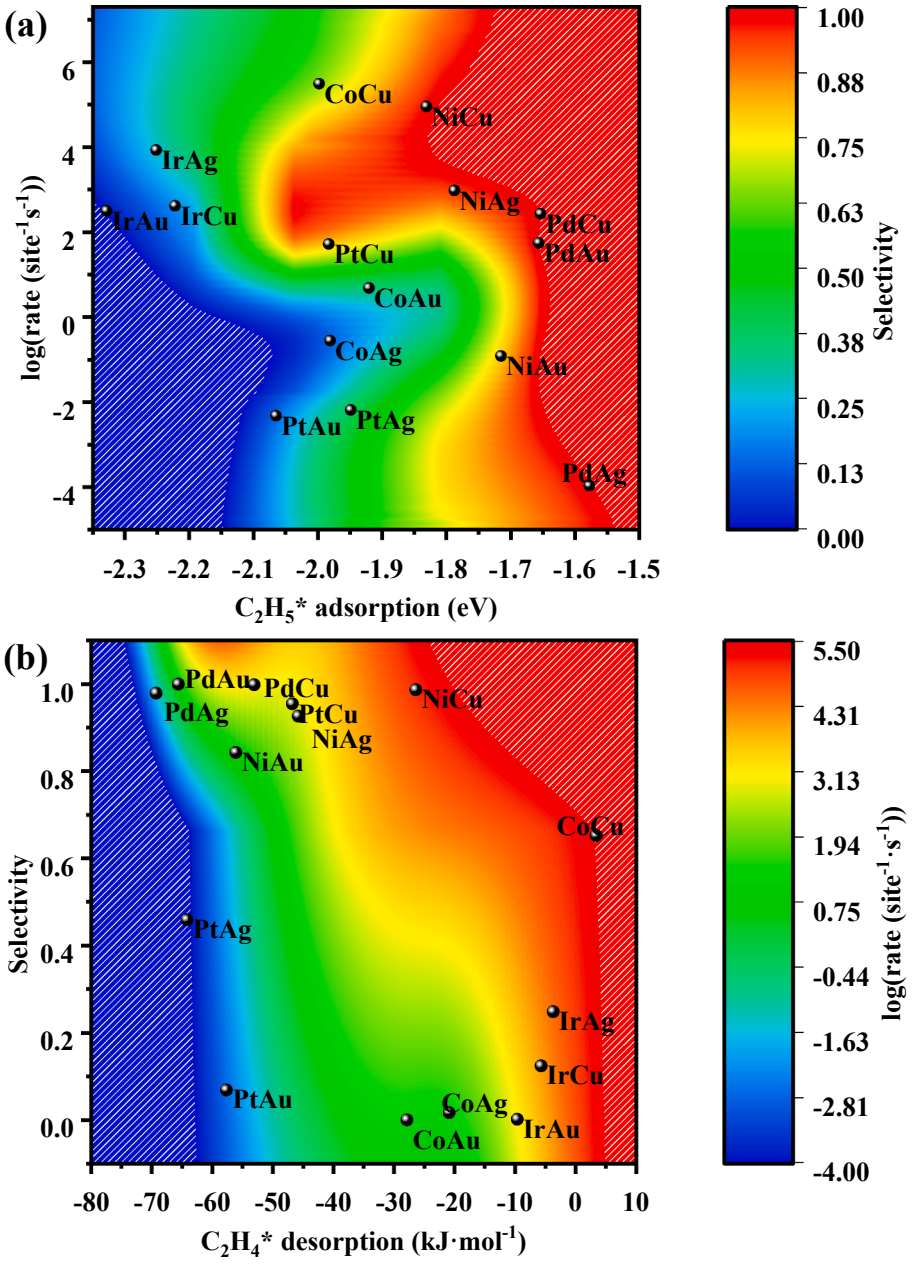

Fig. 9. Relationship of C_2H_4* selectivity and formation rate on the SAA catalysts with (a) the adsorption energy of C_2H_5*, and (b) C_2H_4* desorption energy at 873.15 K and 1 atm. White lines on the edge of the coordinate axis represent the limits of C_2H_4* selectivity and formation rate.

formation rate of C_2H_4* also decreases. CoCu, NiCu, IrAg, NiAg and PdCu showed higher activity of C_2H_4* formation, especially CoCu and NiCu catalyst, which is in agreement with the activity trend results in Section 3.4.1. Previous studies also show that CoCu catalyst has good dehydrogenation activity, for example, Reddy *et al.* [74] showed that CoCu/MgO catalyst with the higher Cu and Co dispersion has better catalytic activity toward the dehydrogenation/dehydration reaction of 1,4-butanediol. Bulut *et al.* [75] prepared CuCo alloy nanoparticles supported on the surface of activated carbon, which showed high activity in the hydrolytic dehydrogenation of ammonia-borane.

Based on above analysis, taking the activity and selectivity of C_2H_4* formation on the SAA catalysts, the NiCu, PdCu and NiAg catalysts are thought to be the promising catalysts in C_2H_6 dehydrogenation, especially, NiCu catalyst.

3.6. Comparisons of catalytic performance between NiCu and Cu, Ag, Au, Pd, Pt, Cr, Pt_3Sn

To further evaluate the performance of NiCu SAA, C_2H_6 dehydrogenation process on the pure Cu, Ag and Au surfaces are investigated (see details in Table 1 and Fig. S5). Firstly, in the desorption process of C_2H_4*, the C–C bond cleavage and the dehydrogenation of C_2H_4* on the Cu, Ag, Au catalysts are kinetically difficult compared to its desorption (151.9, 119.6 *vs.* −68.7, 309.2, 165.2 *vs.* −98.5 and 395.0, 134.3 *vs.* −99.2 kJ·mol^{-1}). Secondly, in the dehydrogenation process of C_2H_5*, the C–C bond cleavage on the Cu, Ag and Au catalysts is also difficult, moreover, Cu, Ag and Au prefer the formation of C_2H_4* in kinetics rather than $CHCH_3$* formation (41.0 *vs.* 82.0, 74.8 *vs.* 158.8 and 109.1 *vs.* 209.1 kJ·mol^{-1}). Finally, in the dehydrogenation process of C_2H_6*, the C–C bond cleavage on the Cu, Ag and Au is difficult compared to its dehydrogenation (132.7 *vs.* 295.4, 196.1 *vs.* 333.6 and 166.7 *vs.* 294.5 kJ·mol^{-1}). Further, microkinetic modeling show that C_2H_4* selectivity on the Cu, Ag and Au catalysts (99.60%, ≈100% and 99.99%) is slightly higher that on NiCu catalyst (98.70%), however, the activity of C_2H_4* formation (9.05×10^4 s^{-1}·site^{-1}) on NiCu is much higher about 4 ~ 13 orders of magnitude than that on the Cu, Ag and Au catalysts (4.84×10^0, 1.42×10^{-8} and 2.18×10^{-9} s^{-1}·site^{-1}). On the other hand, the metal Pd, Pt, Cr and Pt_3Sn catalysts have been widely used in alkane dehydrogenation [17,59,76–78], as a result, C_2H_6 dehydrogenation on the metal Pd, Pt, Cr and Pt_3Sn is further examined to evaluate the catalytic performance of the promising NiCu catalyst (see details in Table 1 and Fig. S4). Firstly, in the desorption process of C_2H_4*, the C–C bond cleavage on the Pd, Pt, Cr and Pt_3Sn catalysts is kinetically difficult; meanwhile, unlike the Pd, Pt and Pt_3Sn catalysts, the Cr catalyst kinetically prefers C_2H_4* dehydrogenation rather than its desorption (33.0 *vs.* 52.1 kJ·mol^{-1}). Secondly, in the dehydrogenation process of C_2H_5*, the C–C bond cleavage on the Pd, Pt, Cr and Pt_3Sn catalysts is also difficult, Pt_3Sn prefers the formation of $CHCH_3$* in kinetics rather than C_2H_4* formation (45.9 *vs.* 66.0 kJ·mol^{-1}). Finally, in the dehydrogenation process of C_2H_6*, the C–C bond cleavage on the Pd, Pt and Pt_3Sn is difficult, while the Cr catalyst kinetically prefers the C–C bond cleavage compared to its dehydrogenation to C_2H_5* (53.4 *vs.* 85.5 kJ·mol^{-1}). Pd and Pt catalysts prefer to produce gas phase C_2H_4 in C_2H_6 dehydrogenation, which agrees with the previously reported studies for C_2H_6 dehydrogenation on the Pt [53] and Pd catalysts [79,80]. In addition, it is noted that previous studies [8,81,82] considered Pt_3Sn catalysts as an excellent catalyst for propane dehydrogenation, in which $CH_3CH = CH_2$(g) selectivity is evaluated only based on the competition between $CH_3CH = CH_2$* dehydrogenation and $CH_3CH = CH_2$* desorption, while the competition between C_3H_7* dehydrogenation to $CH_3CH = CH_2$* and its dehydrogenation to CH_3CH_2CH*/CH_3CCH_3* was not considered. Similarly, for C_2H_6 dehydrogenation, our results also show that C_2H_4* desorption is much easier in kinetics than its dehydrogenation and C–C bond cleavage on Pt_3Sn catalysts, which agrees with that involving in propane dehydrogenation. However, when considering the effect of C_2H_5* dehydrogenation to $CHCH_3$* on $CH_2 = CH_2$* formation, $CHCH_3$* formation is kinetically easier than C_2H_4* formation (45.9 *vs.* 66.0 kJ·mol^{-1}), as a result, C_2H_4 (g) selectivity will decrease. Similar results were also obtained by Nam *et al.* [55], which found that C_2H_5* dehydrogenation to $CHCH_3$* is kinetically favorable than its dehydrogenation to C_2H_4*, namely, $CHCH_3$* formation reduces C_2H_4* selectivity in ethane dehydrogenation on Pt_3Sn catalyst.

As listed in Table S5, among the NiCu, Cu, Ag, Au, Pd and Pt catalysts, the comparisons of catalytic performance show that C_2H_4* selectivity on the Cu, Ag and Au catalysts are close to that on NiCu catalyst, but the activity of C_2H_4* formation are far lower than NiCu catalyst. For Pd and Pt catalysts, C_2H_4* selectivity on NiCu catalyst (98.70%) is close to that on Pd catalyst (99.79%), and is much higher than that on Pt catalyst (43.80%). Meanwhile, the activity of C_2H_4* formation (9.05×10^4 s^{-1}·site^{-1}) on NiCu is higher about 4.6 times than that on Pd catalyst (1.98×10^4 s^{-1}·site^{-1}), and is close to that on Pt catalyst (9.26×10^4 s^{-1}·site^{-1}). Thus, taking the activity and selectivity of C_2H_4* formation on the NiCu, Pd and Pt catalysts, NiCu shows superior catalytic performance than Pd and Pt catalysts. Further, NiCu with the best activity and selectivity is consisted of the non-noble metals Cu as the base materials and Ni as the doped metal, which has a considerable cost advantage compared to the noble metals Pd and Pt. In addition, previous experiments also showed that NiCu catalyst exhibited better catalytic performance toward the dehydrogenation reaction, for example, Luo *et al.* [83] and Janvelyan *et al.* [84] found that the low-cost NiCu bimetallic catalyst exhibited the high-yield and selective production of H_2 and acetaldehyde in ethanol dehydrogenation process. Shan *et al.* [29,85] studied the selective non-oxidative dehydrogenation of ethanol to acetaldehyde and H_2 on highly dilute NiCu alloys, suggesting that adding a small amount of Ni into Cu to form highly dilute NiCu alloys dramatically increases the catalytic activity and their long-term stability.

3.7. Dual descriptors proposed to evaluate the activity and selectivity of C_2H_6 dehydrogenation

Based on above results about two dehydrogenation steps and one desorption step involving in C_2H_6* dehydrogenation to gas phase C_2H_4, the dual descriptors are proposed to evaluate the catalytic activity and selectivity of C_2H_6 dehydrogenation on the single-atom Co, Ir, Ni, Pd and Pt doped-Cu, Ag and Au SAA catalysts: One is the adsorption energy of C_2H_5* defined as the first descriptor to evaluate C_2H_4* selectivity, in which the weaker the adsorption energy of C_2H_5* is, the higher the selectivity of C_2H_4* is. The other is the desorption energy of C_2H_4* defined as the second descriptor to evaluate the activity of C_2H_4* formation, in which the lower the desorption energy of C_2H_4* is, the lower the activity of C_2H_4* formation is.

4. Conclusions

In this work, C_2H_6 dehydrogenation to gas phase C_2H_4 on fifteen types of SAA catalysts including the single-atom Co, Ir, Ni, Pd and Pt doped-Cu, Ag and Au, three pure metal Pd, Pt and Cr, and Pt_3Sn catalysts were fully investigated using DFT calculations and microkinetic modeling. Here, the related reactions involving in the dehydrogenation processes of C_2H_6* and C_2H_5*, and the desorption process of C_2H_4* were considered. The result shows that the dehydrogenation steps of C_2H_6* and C_2H_5* is the rate-determining step of C_2H_6 dehydrogenation to gas phase C_2H_4, the selectivity of gas phase C_2H_4 is mainly controlled by the dehydrogenation of C_2H_5* to form $CHCH_3$* or C_2H_4*. Ten types of SAA catalysts including the CoCu, NiCu, PdCu, PtCu, IrAg, NiAg, PdAg, PtAg, NiAu and PdAu are screened out to favor the formation of gas phase C_2H_4, among them, the low cost NiCu catalyst exhibits the best activity and selectivity toward gas phase C_2H_4 formation, which is superior to the noble metals Pd and Pt widely reported. More importantly, the activity of C_2H_6 dehydrogenation to gas phase C_2H_4 on all considered SAAs catalysts has a relationship with C_2H_4 desorption energy, the easier the desorption of C_2H_4 is, the lower the activity of C_2H_6 dehydrogenation to

gas phase C_2H_4 is. Similarly, C_2H_4 selectivity has a relationship with C_2H_5 adsorption energy, the weaker C_2H_5 adsorption energy is, the higher C_2H_4 selectivity is. Essential reason of the close relationship was explained based on the analysis of electronic properties. Further, the dual descriptors, C_2H_4 desorption energy and C_2H_5 adsorption energy on the catalyst, were proposed to evaluate the activity and selectivity of C_2H_6 dehydrogenation to gas phase C_2H_4, respectively, which could provide a simple and valuable method to screen out high performance SAA catalysts in alkane dehydrogenation to alkene.

CRediT authorship contribution statement

Yuan Zhang: Writing – original draft, Writing - review & editing, Formal analysis. **Baojun Wang:** Writing – original draft, Writing - review & editing, Data curation, Conceptualization, Resources, Funding acquisition, Software, Project administration, Supervision. **Maohong Fan:** Formal analysis. **Debao Li:** Formal analysis. **Riguang Zhang:** Writing – original draft, Writing - review & editing, Data curation, Conceptualization, Funding acquisition, Resources, Supervision.

Declaration of Competing Interest

The authors declare that they have no known competing financial interests or personal relationships that could have appeared to influence the work reported in this paper.

Acknowledgments

This work is financially supported by the Key Projects of National Natural Science Foundation of China (No. 21736007), the National Natural Science Foundation of China (Nos. 21776193 and 22078221).

Appendix A. Supplementary data

Supplementary data to this article can be found online at https://doi.org/10.1016/j.fuel.2021.121641.

References

[1] Bodke AS, Olschki DA, Schmidt LD, Ranzi E. High selectivities to ethylene by partial oxidation of ethane. Science 1999;285:712–5.
[2] Wang GW, Zhu XL, Li CY. Recent progress in commercial and novel catalysts for catalytic dehydrogenation of light alkanes. Chem Rec 2020;20:604–16.
[3] Melzer D, Mestl G, Wanninger K, Zhu YY, Browning ND, Sanchez-Sanchez M, et al. Design and synthesis of highly active MoVTeNb-oxides for ethane oxidative dehydrogenation. Nat Commun 2019;10:4012.
[4] Cao L, Dai PC, Zhu L, Yan LT, Chen RH, Liu DD, et al. Graphitic carbon nitride catalyzes selective oxidative dehydrogenation of propane. Appl Catal B-Environ. 2020;262:118277.
[5] Zhou YL, Lin J, Li L, Tian M, Li XY, Pan XL, et al. Improving the selectivity of Ni-Al mixed oxides with isolated oxygen species for oxidative dehydrogenation of ethane with nitrous oxide. J Catal 2019;377:438–48.
[6] Sattler JJHB, Ruiz-Martinez J, Santillan-Jimenez E, Weckhuysen BM. Catalytic dehydrogenation of light alkanes on metals and metal oxides. Chem Rev 2014;114:10613–53.
[7] Wang LC, Zhang YY, Xu JY, Diao WJ, Karakalos S, Liu B, et al. Non-oxidative dehydrogenation of ethane to ethylene over ZSM-5 zeolite supported iron catalysts. Appl Catal B-Environ 2019;256:117816.
[8] Zha SJ, Sun GD, Wu TF, Zhao JB, Zhao ZJ, Gong JL. Identification of Pt-based catalysts for propane dehydrogenation via a probability analysis. Chem Sci 2018;9:3925–31.
[9] Chen H, Li LL, Hu JL. Upgrading of stranded gas via non-oxidative conversion processes. Catal Today 2018;310:94–7.
[10] Vincent RS, Lindstedt RP, Malik NA, Reid IAB, Messenger BE. The chemistry of ethane dehydrogenation over a supported platinum catalyst. J Catal 2008;260:37–64.
[11] Burch R, Garla LC. Platinum-tin reforming catalysts: II. Activity and selectivity in hydrocarbon reactions. J Catal 1981;71:360–72.
[12] Bariås OA, Holmen A, Blekkan EA. Propane dehydrogenation over supported Pt and Pt–Sn catalysts: Catalyst preparation, characterization, and activity measurements. J Catal 1996;158:1–12.
[13] Peng ZM, Somodi F, Helveg S, Kisielowski C, Specht P, Bell AT. High-resolution in situ and ex situ TEM studies on graphene formation and growth on Pt nanoparticles. J Catal 2012;286:22–9.
[14] Tsai Y-L, Xu C, Koel BE. Chemisorption of ethylene, propylene and isobutylene on ordered Sn/Pt(111) surface alloys. Surf Sci 1997;385(1):37–59.
[15] Zhao HB, Koel BE. Reactivity of ethyl groups on a Sn/Pt(111) surface alloy. Catal Lett 2005;99:27–32.
[16] Zeigarnik AV, Valdés-Pérez RE, Myatkovskaya ON. C−C bond scission in ethane hydrogenolysis. J Phys Chem B 2000;104:10578–87.
[17] Bednarova L, Lyman CE, Rytter E, Holmen A. Effect of support on the size and composition of highly dispersed Pt–Sn particles. J Catal 2002;211:335–46.
[18] Galvita V, Siddiqi G, Sun P, Bell AT. Ethane dehydrogenation on Pt/Mg(Al)O and PtSn/Mg(Al)O catalysts. J Catal 2010;271:209–19.
[19] Batzill M, Beck DE, Koel BE. Electronic contrast in scanning tunneling microscopy of Sn–Pt(111) surface alloys. Surf Sci 2000;466(1-3):L821–6.
[20] Panja C, Saliba NA, Koel BE. Coking resistance of Pt–Sn alloys probed by acetylene chemisorption. Catal Lett 2000;68:175–80.
[21] Panja C, Saliba NA, Koel BE. Acetylene chemisorption on Sn/Pt(100) alloys. J Phys Chem B 2001;105:3786–96.
[22] Kyriakou G, Boucher M, Jewell A, Lewis E, Lawton T, Baber A, et al. Isolated metal atom geometries as a strategy for selective heterogeneous hydrogenations. Science 2012;335:1209–12.
[23] Tierney HL, Baber AE, Kitchin JR, Sykes ECH. Hydrogen dissociation and spillover on individual isolated palladium atoms. Phys Rev Lett 2009;103:246102.
[24] Tierney HL, Baber AE, Sykes ECH. Atomic-scale imaging and electronic structure determination of catalytic sites on Pd/Cu near surface alloys. J Phys Chem C 2009;113:7246–50.
[25] Baber AE, Tierney HL, Lawton TJ, Sykes ECH. An atomic-scale view of palladium alloys and their ability to dissociate molecular hydrogen. ChemCatChem 2011;3:607–14.
[26] Marcinkowski MD, Jewell AD, Stamatakis M, Boucher MB, Lewis EA, Murphy CJ, et al. Controlling a spillover pathway with the molecular cork effect. Nat Mater 2013;12:523–8.
[27] Wang Z-T, Darby MT, Therrien AJ, El-Soda M, Michaelides A, Stamatakis M, et al. Preparation, structure, and surface chemistry of Ni–Au single atom alloys. J Phys Chem C 2016;120(25):13574–80.
[28] Marcinkowski MD, Darby MT, Liu JL, Wimble JM, Lucci FR, Lee S, et al. Pt/Cu single-atom alloys as coke-resistant catalysts for efficient C-H activation. Nat Chem 2018;10:325–32.
[29] Shan JJ, Liu JL, Li MW, Lustig S, Lee S, Flytzani-Stephanopoulos M. NiCu single atom alloys catalyze the C-H bond activation in the selective non-oxidative ethanol dehydrogenation reaction. Appl. Catal. B-Environ. 2018;226:534–43.
[30] Jiang Z, Wu ZQ, Fang T, Yi CH. Enhancement C-H bond activation of methane via doping Pd, Pt, Rh and Ni on Cu(111) surface: A DFT study. Chem Phys Lett 2019;715:323–9.
[31] Darby MT, Réocreux R, Sykes ECH, Michaelides A, Stamatakis M. Elucidating the stability and reactivity of surface intermediates on single-atom alloy catalysts. ACS Catal 2018;8:5038–50.
[32] Li H, Chai WR, Henkelman G. Selectivity for ethanol partial oxidation: The unique chemistry of single-atom alloy catalysts on Au, Ag, and Cu(111). J Mater Chem A 2019;7:23868–77.
[33] Cao XR. Insight into mechanism and selectivity of propane dehydrogenation over the Pd-doped Cu(111) surface. RSC Adv 2016;6:65524–32.
[34] Sun GD, Zhao ZJ, Mu RT, Zha SJ, Li LL, Chen S, et al. Breaking the scaling relationship via thermally stable Pt/Cu single atom alloys for catalytic dehydrogenation. Nat Commun 2018;9:4454.
[35] Réocreux R, Kress PL, Hannagan RT, Çınar V, Stamatakis M, Sykes ECH. Controlling hydrocarbon (de)hydrogenation pathways with bifunctional PtCu single-atom alloys. J Phys Chem Lett 2020;11(20):8751–7.
[36] Xu L, Stangland EE, Mavrikakis M. Ethylene versus ethane: A DFT-based selectivity descriptor for efficient catalyst screening. J Catal 2018;362:18–24.
[37] Pérez-Ramírez J, López N. Strategies to break linear scaling relationships. Nat Catal 2019;2:971–6.
[38] Tkatchenko A. Machine learning for chemical discovery. Nat Commun 2020;11:4125.
[39] Kohn W, Becke AD, Parr RG. Density functional theory of electronic structure. J Phys Chem 1996;100:12974–80.
[40] Perdew JP, Burke K, Ernzerhof M. Generalized gradient approximation made simple. Phys Rev Lett 1996;77:3865–8.
[41] Blöchl PE. Projector augmented-wave method. Phys. Rev. B 1994;50(24):17953–79.
[42] Kresse G, Joubert D. From ultrasoft pseudopotentials to the projector augmented-wave method. Phys. Rev. B 1999;59:1758–75.
[43] Monkhorst HJ, Pack JD. Special points for brillouin-zone integrations. Phys. Rev. B 1976;13:5188–92.
[44] Grimme S, Antony J, Ehrlich S, Krieg H. A consistent and accurate ab initio parametrization of density functional dispersion correction (DFT-D) for the 94 elements H-Pu. J Chem Phys 2010;132:154104.
[45] Henkelman G, Uberuaga BP, Jónsson H. A climbing image nudged elastic band method for finding saddle points and minimum energy paths. J Chem Phys 2000;113:9901–4.
[46] Henkelman G, Jónsson H. Improved tangent estimate in the nudged elastic band method for finding minimum energy paths and saddle points. J Chem Phys 2000;113:9978–85.
[47] Henkelman G, Jónsson H. A dimer method for finding saddle points on high dimensional potential surfaces using only first derivatives. J Chem Phys 1999;111:7010–22.

[48] Wang V, Xu N, Liu JC, Tang G, Geng WT. VASPKIT: A user-friendly interface facilitating high-throughput computing and analysis using VASP code. Comput Phys Commun 2021;267:108033.
[49] Hansen MH, Nørskov JK, Bligaard T. First principles micro-kinetic model of catalytic non-oxidative dehydrogenation of ethane over close-packed metallic facets. J Catal 2019;374:161–70.
[50] Maeno Z, Yasumura S, Wu XP, Huang MW, Liu C, Toyao T, et al. Isolated indium-hydrides in cha zeolites: Speciation and catalysis for nonoxidative dehydrogenation of ethane. J Am Chem Soc 2020;142:4820–32.
[51] Bian YX, Kim M, Li T, Asthagiri A, Weaver JF. Facile dehydrogenation of ethane on the IrO_2(110) surface. J Am Chem Soc 2018;140:2665–72.
[52] Hook A, Celik FE. Predicting selectivity for ethane dehydrogenation and coke formation pathways over model Pt-M surface alloys with ab initio and scaling methods. J Phys Chem C 2017;121:17882–92.
[53] Chen Y, Vlachos DG. Hydrogenation of ethylene and dehydrogenation and hydrogenolysis of ethane on Pt(111) and Pt(211): A density functional theory study. J Phys Chem C 2010;114:4973–82.
[54] Lian Z, Ali S, Liu TF, Si CW, Li B, Su DS. Revealing the janus character of the coke precursor in the propane direct dehydrogenation on Pt catalysts from a kMC simulation. ACS Catal 2018;8:4694–704.
[55] Nam J, Celik FE. Effect of tin in the bulk of platinum-tin alloys for ethane dehydrogenation. Top Catal 2020;63:700–13.
[56] Chang QY, Wang KQ, Hu P, Sui ZJ, Zhou XG, Chen D, et al. Dual-function catalysis in propane dehydrogenation over Pt_1–Ga_2O_3 catalyst: Insights from a microkinetic analysis. AIChE J 2020;66:e16232.
[57] Cao XM, Burch R, Hardacre C, Hu P. An understanding of chemoselective hydrogenation on crotonaldehyde over Pt(111) in the free energy landscape: The microkinetics study based on first-principles calculations. Catal Today 2011;165:71–9.
[58] Saelee T, Namuangruk S, Kungwan N, Junkaew A. Theoretical insight into catalytic propane dehydrogenation on Ni(111). J Phys Chem C 2018;122:14678–90.
[59] Yang ML, Zhu YA, Fan C, Sui ZJ, Chen D, Zhou XG. DFT study of propane dehydrogenation on Pt catalyst: Effects of step sites. PCCP 2011;13(8):3257. https://doi.org/10.1039/c0cp00341g.
[60] Hook A, Massa JD, Celik FE. Effect of tin coverage on selectivity for ethane dehydrogenation over platinum–tin alloys. J Phys Chem C 2016;120:27307–18.
[61] Latimer AA, Kulkarni AR, Aljama H, Montoya JH, Yoo JS, Tsai C, et al. Understanding trends in C-H bond activation in heterogeneous catalysis. Nat Mater 2017;16:225–9.
[62] Zhao ZJ, Liu SH, Zha SJ, Cheng DF, Studt F, Henkelman G, et al. Theory-guided design of catalytic materials using scaling relationships and reactivity descriptors. Nat Rev Mater 2019;4:792–804.
[63] Zhao ZJ, Zhao JB, Chang X, Zha SJ, Zeng L, Gong JL. Competition of C-C bond formation and C-H bond formation for acetylene hydrogenation on transition metals: A density functional theory study. AIChE J 2019;65:1059–66.
[64] Studt F, Sharafutdinov I, Abild-Pedersen F, Elkjær CF, Hummelshøj JS, Dahl S, et al. Discovery of a Ni-Ga catalyst for carbon dioxide reduction to methanol. Nat Chem 2014;6:320–4.
[65] Fung V, Hu G, Sumpter B. Electronic band contraction induced low temperature methane activation on metal alloys. J Mater Chem A 2020;8:6057–66.
[66] Thirumalai H, Kitchin JR. Investigating the reactivity of single atom alloys using density functional theory. Top Catal 2018;61:462–74.
[67] Nørskov JK, Studt F, Abildpedersen F, Bligaard T. Fundamental Concepts in Heterogeneous Catalysis. Hoboken: John Wiley & Sons; 2014. p. 114–37.
[68] Nørskov JK, Bligaard T, Rossmeisl J, Christensen CH. Towards the computational design of solid catalysts. Nat Chem 2009;1:37–46.
[69] Medford AJ, Vojvodic A, Hummelshøj JS, Voss J, Abild-Pedersen F, Studt F, et al. From the sabatier principle to a predictive theory of transition-metal heterogeneous catalysis. J Catal 2015;328:36–42.
[70] Hulva J, Meier M, Bliem R, Jakub Z, Kraushofer F, Schmid M, et al. Unraveling CO adsorption on model single-atom catalysts. Science 2021;371:375–9.
[71] Wang W, Wang Ye, Wang G-C. Ethanol synthesis from syngas over Cu(Pd)-doped Fe(100): A systematic theoretical investigation. PCCP 2018;20(4):2492–507.
[72] Steinberg S, Dronskowski R. The crystal orbital hamilton population (COHP) method as a tool to visualize and analyze chemical bonding in intermetallic compounds. Crystals 2018;8:225.
[73] Niu H, Wang X, Shao C, Liu Y, Zhang Z, Guo Y. Revealing the oxygen reduction reaction activity origin of single atoms supported on g-C_3N_4 monolayers: A first-principles study. J Mater Chem A 2020;8(14):6555–63.
[74] Reddy KHP, Anand N, Prasad PSS, Rao KSR, Raju BD. Influence of method of preparation of Co-Cu/MgO catalyst on dehydrogenation/dehydration reaction pathway of 1, 4-butanediol. Catal Commun 2011;12(10):866–9.
[75] Bulut A, Yurderi M, Ertas İE, Celebi M, Kaya M, Zahmakiran M. Carbon dispersed copper-cobalt alloy nanoparticles: A cost-effective heterogeneous catalyst with exceptional performance in the hydrolytic dehydrogenation of ammonia-borane. Appl. Catal. B-Environ. 2016;180:121–9.
[76] Olsbye U, Virnovskaia A, Prytz Ø, Tinnemans SJ, Weckhuysen BM. Mechanistic insight in the ethane dehydrogenation reaction over Cr/Al_2O_3 catalysts. Catal Lett 2005;103:143–8.
[77] Fu BS, Lu JL, Stair PC, Xiao GM, Kung MC, Kung HH. Oxidative dehydrogenation of ethane over alumina-supported pd catalysts. Effect of alumina overlayer. J Catal 2013;297:289–95.
[78] Hu ZP, Wang Z, Yuan ZY. Cr/Al_2O_3 catalysts with strong metal-support interactions for stable catalytic dehydrogenation of propane to propylene. Mol Catal 2020;493:111052.
[79] Chen Z-X, Aleksandrov HA, Basaran D, Rösch N. Transformations of ethylene on the Pd(111) surface: A density functional study. J Phys Chem C 2010;114(41):17683–92.
[80] Wu ZW, Wegener EC, Tseng HT, Gallagher JR, Harris JW, Diaz RE, et al. Pd–In intermetallic alloy nanoparticles: Highly selective ethane dehydrogenation catalysts. Catal Sci Technol 2016;6:6965–76.
[81] Yang ML, Zhu YA, Zhou XG, Sui ZJ, Chen D. First-principles calculations of propane dehydrogenation over PtSn catalysts. ACS Catal 2012;2:1247–58.
[82] Nykänen L, Honkala K. Selectivity in propene dehydrogenation on Pt and Pt_3Sn surfaces from first principles. ACS Catal 2013;3:3026–30.
[83] Luo SQ, Song H, Philo D, Oshikiri M, Kako T, Ye JH. Solar-driven production of hydrogen and acetaldehyde from ethanol on Ni-Cu bimetallic catalysts with solar-to-fuels conversion efficiency up to 3.8 %. Appl. Catal. B-Environ. 2020;272:118965.
[84] Janvelyan N, van Spronsen MA, Wu CH, Qi Z, Montemore MM, Shan J, et al. Stabilization of a nanoporous NiCu dilute alloy catalyst for non-oxidative ethanol dehydrogenation. Catal Sci Technol 2020;10:5207–17.
[85] Shan JJ, Janvelyan N, Li H, Liu JL, Egle TM, Ye JC, et al. Selective non-oxidative dehydrogenation of ethanol to acetaldehyde and hydrogen on highly dilute NiCu alloys. Appl Catal B-Environ 2017;205:541–50.